Dynamic Frequency Support and DC Voltage Regulation Approach for VSC-MTDC Systems

Chongru Liu, *Senior Member*, *IEEE*, *Senior Member*, *CSEE*, Haoyu Liu, Siwen Jiang, *Student Member*, *IEEE*, and Le Zheng, *Member*, *IEEE*, *Member*, *CSEE*

***Abstract*—When an additional frequency control is implemented in the voltage source converter-based multi-terminal high voltage direct current (VSC-MTDC) system, the DC grid is capable of responding to a frequency disturbance in the AC system. However, the original additional frequency control may cause the DC voltage to exceed the limit when providing power for a severe frequency disturbance, threatening the security of the DC system. A novel dynamic additional frequency control strategy for the VSC-MTDC system is developed based on the relationship between the DC voltage and the frequency droop coefficient. A dynamic frequency droop coefficient is designed to adaptively adjust the support power of the DC grid, balancing the frequency regulation of the disturbed AC system and the voltage stability of the DC grid. A DC voltage recovery method based on multi-converter cooperation is proposed to cope with the DC voltage deviation caused by the additional frequency control. Simulations validate the advantages and satisfactory performance of the proposed method during power disturbances with different severities and for the process of DC voltage recovery.**

***Index Terms*—Additional frequency control, DC voltage recovery module, dynamic frequency droop coefficient, VSC-MTDC.**

I. Introduction

COMPARED with the traditional line-commutated converter high voltage direct current (LCC-HVDC), flexible HVDC based on voltage source converters (VSC) or modular multilevel converters (MMC) have been more widely used due to the advantages of decoupled active/reactive power control and no commutation failures [1]–[3]. VSC-MTDC technology, with different operational modes, has gained significance in enabling large-scale clean energy consumption and remote offshore wind power transmission [4]–[6]. Maintaining the frequency stability of the AC system is an important task of AC/DC hybrid systems. Therefore, it is of great significance to investigate the power support capability of the VSC-MTDC system to improve the frequency stability when the AC system is disturbed.

Manuscript received May 12, 2021; revised June 1, 2021; accepted August 6, 2021. Date of online publication January 5, 2022; date of current version September 22, 2022. This work was supported by the Science and Technology Project of SGCC (SGZJ0000KXJS1900419).

C. R. Liu, H. Y. Liu, S. W. Jiang and L. Zheng (corresponding author, email: zhengl20@ncepu.edu.cn) are with the State Key Laboratory for Alternate Electrical Power System with Renewable Energy Sources, North China Electric Power University, Beijing 102206, China.

DOI: 10.17775/CSEEJPES.2021.01790

The control modes of a VSC-MTDC system primarily include master-slave control, margin control, droop control and nonlinear control. The master-slave control and margin control [7] are the operational modes in which a single station absorbs the unbalanced power during a certain time, so that the VSCs can easily reach the power limit. Nonlinear control [8], [9] has good control performance and strong robustness, but the design is more complex and the engineering application is less. The droop control [10] is easy to design, and multiple VSCs undertake unbalanced power at the same time, which has been widely used in real-world applications.

Due to the limitations of the control system of VSC-MTDC, frequency disturbances occurring in one AC system are difficult to be transmitted to the other connected AC systems via the MTDC system. The frequency regulation ability only depends on the inertia and primary frequency regulation of the disturbed AC system. The power support capability of the connected AC systems has been severely weakened.

Therefore, an additional frequency controller is proposed to be superimposed on the droop controller to transfer the frequency disturbance through the MTDC system to the connected AC systems. According to this idea, there are several different alternatives: 1) The output of the frequency droop controller is superimposed on the reference value of the active power of droop control, as proposed in [11] and [12]; 2) The output of the frequency outer loop is superimposed on the reference value of the DC voltage to achieve a similar effect in [13]–[15]; 3) A hybrid control strategy is proposed, as in [16], which switches the VSC control mode among the active power versus the DC voltage, active power versus the frequency, and DC voltage versus the frequency based on a specific parameter matrix.

Compared with the conventional AC source, the offshore wind turbine using maximum power point tracking (MPPT) cannot apply rotational kinetic energy to participate in the frequency regulation of the onshore AC system; except when establishing the droop relationship, as in [13], between the DC voltage and frequency for the grid-side VSC and the offshore AC system, [17] and in [18] which designed a frequency-active power droop loop based on MPPT to respond to frequency disturbances in the onshore AC system. Whether the MTDC system connected to the conventional AC source or the wind farm, the additional frequency control [11]–[18] only considered the basic frequency support function, and the control structure needs to be optimized.

To maintain stability of the control system and improve frequency support capability of the MTDC system, several researchers developed improved additional frequency control methods. In [19] and [20], an operation dead-band was designed for additional frequency control to prevent the AC/DC system from repeatedly fluctuating due to the frequent action of the additional frequency control. According to the principle of grading and districting, the start-up sequence of the additional frequency control under different operating conditions was formulated to suppress the frequency deviation [21]. The frequency droop coefficient was interconnected with the frequency variation, and the MTDC support power was automatically adjusted according to the frequency deviation of the AC system [22]. In [23] and [24], the frequency deviation and the rate of change of frequency (RoCoF) of each AC system were transmitted using interstation communication, thus achieving integrated frequency regulation of the entire AC/DC system. Reference [25] exploited MPPT and employed the frequency deviation and the RoCoF to generate an active power reference increment to emulate the inertia.

In contrast to the additional frequency control based on droop control, researchers [26]–[30] proposed other frequency regulation methods. Reference [26] used the damping coefficient to establish the droop relationship between the active power and frequency based on the virtual synchronous generator control (VSG), so that the VSC could respond to the AC system frequency disturbance. Several researchers [27]–[29] combined VSG with additional frequency control for frequency regulation by using a collaborative control of the frequency deviation and the RoCoF. In [30], the incremental reference value of the MMC capacitance energy management system was proportional to the local measured frequency deviation and the RoCoF; thus, an indirect relationship between the frequency and DC voltage was established to support the short-term primary frequency regulation and emulate the inertia.

In addition, PI gains have a significant impact on the operation performance of droop control. An improved meta-heuristic algorithm [31] employs multiple classes, and enables teachers or students from different classes interactive learning through a small world network, thus effectively avoiding the local optimal problem in the optimization process. The method can obtain excellent optimization results in PI gain tuning.

Present additional frequency control methods of VSC-MTDC systems generally focus on improving the ability of the MTDC system to suppress the frequency offset during power disturbances. However, when the additional frequency control provides power support for a large frequency deviation, the DC voltage may exceed the stable operation range, thus affecting the safety and economic operations of the entire MTDC system. The DC voltage control loop based on proportional-integral (PI) control can partly cope with the DC voltage deviation caused by the additional frequency control [32]. The essence of the DC voltage recovery is to change the VSC control mode to a fixed voltage control, which does not fully exploit the coordination ability of the droop control, and results in violent power fluctuations at the moment of implementation. Therefore, maintaining the DC voltage stability as well as developing a preferable DC voltage recovery method at the time of the AC side frequency regulation is an urgent need.

This paper improves the original additional frequency control [11], and proposes a novel dynamic additional frequency control strategy to avoid the DC voltage seriously deviating when regulating frequency and implementing the DC voltage recovery. The main contributions of this paper are:

1) Analyzsing the relationship between frequency and DC voltage when the VSC-MTDC system implements the additional frequency control.

2) Designing the dynamic frequency droop coefficient and implementing stability analysis. The dynamic frequency droop coefficient can adaptively adjust according to the change of the frequency and the DC voltage deviation caused by frequency disturbance to balance the frequency regulation of the disturbed AC system and the DC voltage stability of the DC grid under various power contingencies.

3) Developing a DC voltage recovery strategy based on multi-converter coordination to implement the DC voltage non-error recovery. The DC voltage recovery gain in the form of the Butterworth function is designed to fulfill the smooth connection of the DC voltage recovery module to the control system and avoid power oscillations.

The remainder of this paper is organized as follows. Section II provides a brief introduction of the original additional frequency control and describes the structure of the proposed novel dynamic additional frequency control strategy. The dynamic frequency control module is designed in Section III. Section IV develops the DC voltage recovery method. The proposed strategy is validated on a four-terminal VSC system in Section V. Section VI concludes this paper.

II. A Novel Additional Frequency Control

A. The Original Additional Frequency Control

The structure of the original additional frequency control is shown in Fig. 1. U_{dc} and U_{dcref} represent the actual and reference values of the DC voltage of the VSC, respectively. P and P^{*}_{ref} represent the actual and reference values of the active power transmitted by the VSC, respectively. f and f^{*} represent the actual and reference values of the AC system frequency, respectively, and Δf is the frequency deviation. ΔP_{ref} represents the incremental active power value generated by the additional frequency control. K_{f} is the frequency droop coefficient, K_{V} is the DC voltage droop coefficient. K_p and K_i are the PI control parameters of the VSC active power

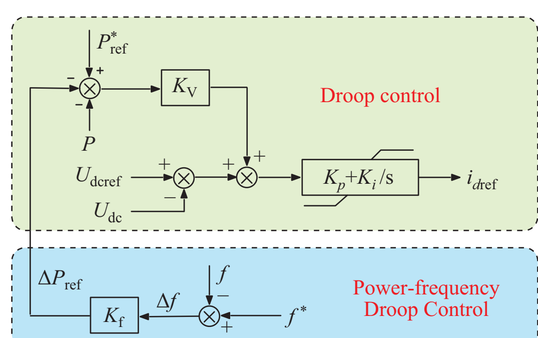

Fig. 1. Control block for the original additional frequency control.

outer loop, respectively. i_{dref} is the current reference value on the d-axis.

The frequency droop loop of additional frequency control adds the increment of the power reference value caused by the frequency deviation to the steady-state power reference value of the VSC droop control; thus, transmitting the frequency change of the disturbed AC system to the voltage change of the DC grid and ensure that the normal converters provide power support.

B. DC Voltage Deviation Caused by Frequency Disturbance

It can be seen from Fig. 1 that the $U_{\mathrm{dc}} - P$ characteristics with additional frequency control can be represented by (1):

$$(U_{\mathrm{dcref}} - U_{\mathrm{dc}}) + K_{\mathrm{V}}\left(P_{\mathrm{ref}} - P\right) = 0 \tag{1}$$

where P_{ref} represents the actual reference value of the active power, which is composed of two parts:

$$P_{\mathrm{ref}} = P_{\mathrm{ref}}^{*} - \Delta P_{\mathrm{ref}} \tag{2}$$

The characteristic of the $f - \Delta P_{\mathrm{ref}}$ corresponding to the additional frequency control is defined in (3):

$$\Delta P_{\mathrm{ref}} = K_{\mathrm{f}}(f^{*} - f) \tag{3}$$

Substituting (1) with (2) and (3):

$$(P_{\mathrm{ref}}^{*} - P) = -\frac{1}{K_{\mathrm{V}}}\left(U_{\mathrm{dcref}} - U_{\mathrm{dc}}\right) + K_{\mathrm{f}}\left(f^{*} - f\right) \tag{4}$$

which can be written as:

$$\Delta P = -\frac{1}{K_{\mathrm{V}}}\Delta U_{\mathrm{dc}} + K_{\mathrm{f}}\Delta f \tag{5}$$

where $\Delta P = P_{\mathrm{ref}}^{*} - P$, $\Delta U_{\mathrm{dc}} = U_{\mathrm{dcref}} - U_{\mathrm{dc}}$, and $\Delta f = f^{*} - f$.

Due to the power losses in the DC grid, the VSCs cannot initially operate at the desired active power and DC voltage point. The initial active power of VSC$_i$ is:

$$P_i^0 = U_{\mathrm{dc}i}^0 \times \left(\sum \frac{U_{\mathrm{dc}i}^0 - U_{\mathrm{dc}j}^0}{R_{ij}}\right) \tag{6}$$

where $U_{\mathrm{dc}i}^0$ represents the DC voltage of VSC$_i$ at the initial time, R_{ij} is the resistance between two interconnected converters VSC$_i$ and VSC$_j$, and $i = 1, \cdots, n$.

Assuming that the initial AC system frequency is rated, thus the additional frequency control and the DC voltage droop control satisfy the condition:

$$K_{\mathrm{V}i}\Delta P_i^0 + \Delta U_{\mathrm{dc}i}^0 = 0 \tag{7}$$

where $\Delta P_i^0 = P_{\mathrm{ref}}^{*} - P_i^0$ and $\Delta U_{\mathrm{dc}i}^0 = U_{\mathrm{dcref}} - U_{\mathrm{dc}i}^0$, $i = 1, \cdots, n$.

P_i^0 and $U_{\mathrm{dc}i}^0$ can be obtained by solving (6) and (7) using a numerical method.

Following the energy conservation of the MTDC system:

$$\left(\sum_{i=1}^{n} P_i^0\right) + P_{\mathrm{loss}} = 0 \tag{8}$$

where P_{loss} represents the power losses of the DC grid.

Substituting ΔP_i^0 for P_i^0 in (8) yields:

$$P_{\mathrm{loss}} = \sum_{i=1}^{n} \Delta P_i^0 \tag{9}$$

It is assumed that the VSC$_1$ performs additional frequency control when AC system 1 experiences a power disturbance, whereas the VSCs connected to the remaining $n-1$ normal AC systems maintain the droop control mode. Further neglecting the evolution of P_{loss} in the dynamic process, the ΔU_{dc} of each VSC is equal.

For VSC$_1$, the following applies:

$$\Delta P_1^0 + \Delta P_1^1 = -\frac{1}{K_{\mathrm{V}1}}\left(\Delta U_{\mathrm{dc}1}^0 + \Delta U_{\mathrm{dc}1}\right) + K_{\mathrm{f}1}\Delta f_1 \tag{10}$$

The remaining VSCs satisfy (11):

$$\Delta P_j^0 + \Delta P_j^1 = -\frac{1}{K_{\mathrm{V}j}}\left(\Delta U_{\mathrm{dc}j}^0 + \Delta U_{\mathrm{dc}1}\right) \tag{11}$$

where $\Delta P_j^1 = P_j^0 - P_j^1$, P_j^1 is the steady-state active power of VSC$_j$ after the disturbance, and $j = 2, \cdots, n$. The average value of the DC grid voltage deviation after disturbance $\Delta U_{\mathrm{dc}1}$ is used to approximate the $\Delta U_{\mathrm{dc}i}^1$ of the VSC$_i$, $i = 1, \cdots, n$.

Sum the active power of n VSCs, according to (9), (10) and (11), the DC grid voltage variation would be (12):

$$\Delta U_{\mathrm{dc}} = \frac{1}{\sum_{i=1}^{n}\frac{1}{K_{\mathrm{V}i}}}\left(-P_{\mathrm{loss}} + K_{\mathrm{f}1}\Delta f_1\right) \tag{12}$$

It can be seen from (12) that the DC voltage deviation ΔU_{dc} of the MTDC system is proportional to the frequency droop coefficient K_{f} of the disturbed AC system. For frequency disturbances with different severities, the unbalanced power transmitted to the DC grid can be controlled by adjusting K_{f} of the VSC, which provides an opportunity to achieve the balance between frequency regulation and DC voltage stability.

C. A Novel Dynamic Additional Frequency Control

A novel dynamic additional frequency control of the VSC-MTDC system is proposed to balance the frequency regulation of the disturbed AC system and the DC voltage stability of the MTDC system simultaneously.

The block of the proposed novel dynamic additional frequency control is shown in Fig. 2. f_{h} and f_{l} are the upper and lower thresholds of the novel dynamic additional frequency control, respectively. T is the time constant of the first-order inertial link. K is the proportional gain of the DC voltage recovery module.

The novel dynamic additional frequency control system consists of a droop control module, frequency control module, and DC voltage recovery module. The three parts operate in conjunction to maintain the stability of the DC voltage and the frequency of the connected AC systems.

1) The droop control module is the main component of the VSC-MTDC system control and maintains the energy balance and DC voltage stability of the MTDC system. The frequency control module and DC voltage recovery module are attached to the droop control module.

2) The frequency control module is used to adjust the system frequency when power disturbances occur. It superimposes the power increment caused by the frequency deviation of the disturbed AC system on the reference value of the VSC active

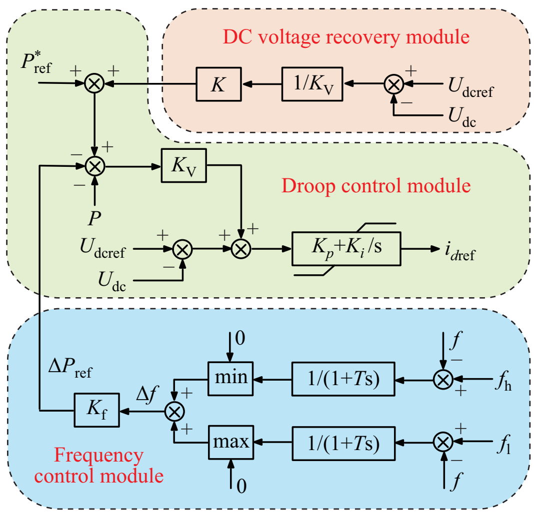

Fig. 2. Control block for the novel dynamic additional frequency control.

power outer-loop control. It then uses the DC voltage deviation to ensure that the MTDC system provides power support. The dynamic additional frequency control adjusts the power support of the DC grid by adaptively adjusting the K_f in the frequency control module, balancing the frequency regulation of the disturbed AC system and the voltage stability of the DC grid to achieve the safe operation of the VSC-MTDC system. The details are described in Section III.

3) The DC voltage recovery module uses the support ability of the connected AC systems to recover the DC voltage after a disturbance. It adds the product of the DC voltage deviation and proportional gain to the active power reference value of the droop control, thus completing DC voltage recovery based on the multi-converter cooperation. The details are described in Section IV.

This paper primarily focuses on the design of the dynamic frequency droop coefficient and the DC voltage recovery gain. The PI parameters of droop control are tuned and optimized according to [33] to meet the requirements for stable operation of the system.

Figure 3 shows the start-up sequence of the three modules for the novel dynamic additional frequency control. At the initial time, only the droop control module works. Once the power disturbance is detected, the frequency control module of the VSC connected to the disturbed AC system goes into action to regulate the frequency. When the DC voltage recovery starts, the VSC connected to the disturbed AC system changes to the fixed active power control and the VSCs connected to normal AC systems implement the DC voltage recovery module.

III. Dynamic Frequency Control Module

A. Design of the Dynamic Frequency Droop Coefficient

Figure 4 shows the design idea for the dynamic frequency droop coefficient. When the AC system suffers from power disturbance, the frequency of the disturbed AC system and the DC network voltage will be affected under the action of the additional frequency control. In order to maintain frequency

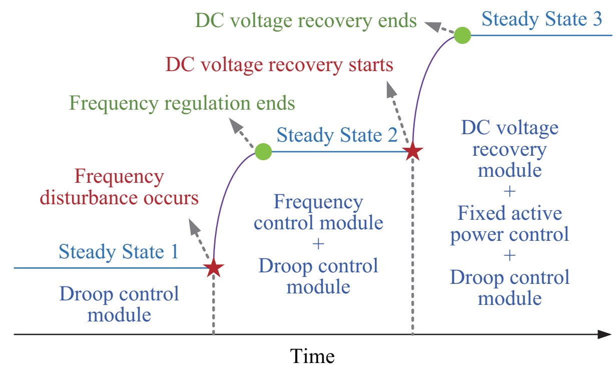

Fig. 3. Start-up sequence of the novel dynamic additional frequency control.

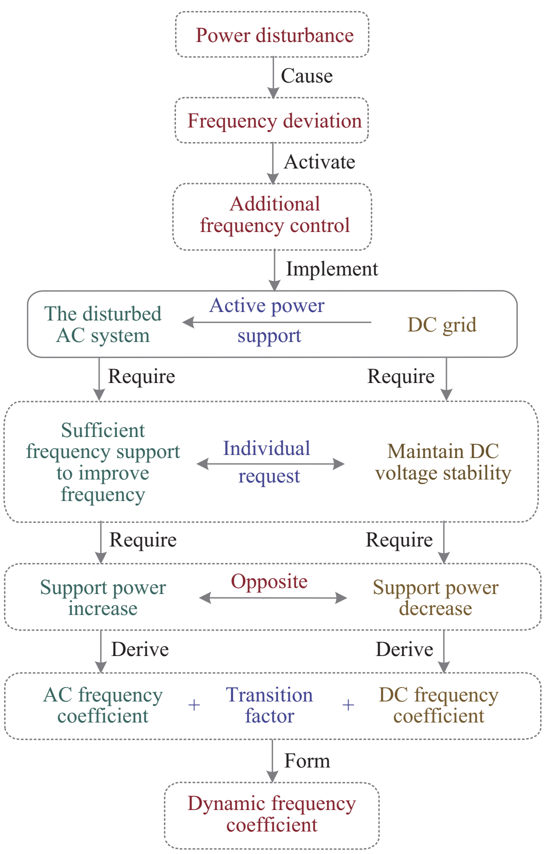

Fig. 4. Idea of the dynamic frequency droop coefficient.

stability, the disturbed AC system needs to obtain sufficient power support, which means that the active power support of the DC grid to the disturbed AC system should be increased. However, the DC grid wants to reduce the support power so as to maintain the stability of the DC voltage. Therefore, the disturbed AC system and the DC grid have contradictions with the demand of the active power support. According to the analysis of Section II-B, the support power is primarily affected by the frequency droop coefficient. Therefore, the AC and the DC frequency droop coefficients are designed respectively to satisfy the power support requirements of the disturbed AC system and DC grid. Moreover, a transition factor is used to transform the two droop coefficients into the dynamic frequency droop coefficient. Thus, the dynamic frequency droop coefficient can adapt to power disturbances with different severities and achieve the coordinated control of the AC frequency and the DC voltage.

The definition of the AC frequency droop coefficient $K_{\mathrm{f}}^{\mathrm{AC}}$ is:

$$K_{\mathrm{f}}^{\mathrm{AC}}=\begin{cases} K_{\mathrm{f0}}^{\mathrm{AC}}+\frac{K_{\mathrm{fmax}}^{\mathrm{AC}}-K_{\mathrm{f0}}^{\mathrm{AC}}}{\Delta f_{\max}}\Delta f & \Delta f\le\Delta f_{\max} \\ K_{\mathrm{fmax}}^{\mathrm{AC}} & \Delta f>\Delta f_{\max}\end{cases} \quad (13)$$

where $K_{\mathrm{fmax}}^{\mathrm{AC}}$ and $K_{\mathrm{f0}}^{\mathrm{AC}}$ represent the maximum and the initial AC frequency droop coefficient, respectively, and $\Delta f_{\max}$ represents the maximum frequency deviation. The AC frequency droop coefficient $K_{\mathrm{f}}^{\mathrm{AC}}$ reflects the demand of the disturbed AC system for DC grid frequency support. The characteristics of $K_{\mathrm{f}}^{\mathrm{AC}}$ are shown in Fig. 5.

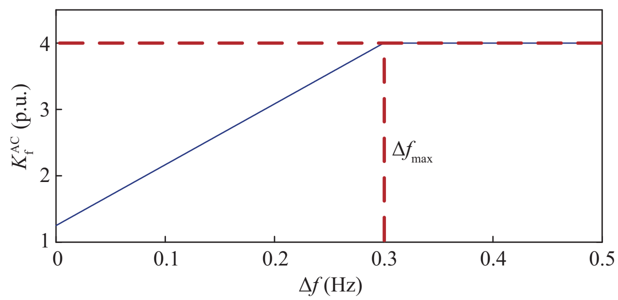

Fig. 5. AC frequency droop coefficient.

The AC frequency droop coefficient $K_{\mathrm{f}}^{\mathrm{AC}}$ increases with an increase in Δf; thus, the unbalanced power transmitted to the DC grid is increased to satisfy the frequency stability requirements of the disturbed AC system. Once Δf exceeds the threshold, $K_{\mathrm{f}}^{\mathrm{AC}}$ remains at the maximum to limit the impact of the large frequency deviation of the AC system on the DC grid.

The DC frequency droop coefficient $K_{\mathrm{f}}^{\mathrm{DC}}$ is defined as:

$$K_{\mathrm{f}}^{\mathrm{DC}}=\begin{cases} K_{\mathrm{f0}}^{\mathrm{DC}}-\frac{K_{\mathrm{f0}}^{\mathrm{DC}}-K_{\mathrm{fmin}}^{\mathrm{DC}}}{\Delta U_{\mathrm{dc\,max}}}\Delta U_{\mathrm{dc}} & \Delta U_{\mathrm{dc}}\le\Delta U_{\mathrm{dcmax}} \\ K_{\mathrm{fmin}}^{\mathrm{DC}} & \Delta U_{\mathrm{dc}}>\Delta U_{\mathrm{dcmax}}\end{cases} \quad (14)$$

where $K_{\mathrm{fmin}}^{\mathrm{DC}}$ and $K_{\mathrm{f0}}^{\mathrm{DC}}$ represent the minimum and initial DC frequency droop coefficient, respectively, and $\Delta U_{\mathrm{dcmax}}$ represents the maximum DC voltage deviation. The DC frequency droop coefficient $K_{\mathrm{f}}^{\mathrm{DC}}$ represents the potential of the DC grid to support the frequency regulation of the disturbed AC system. The characteristics of $K_{\mathrm{f}}^{\mathrm{DC}}$ are shown in Fig. 6.

The DC frequency droop coefficient $K_{\mathrm{f}}^{\mathrm{DC}}$ decreases with an increase in the DC voltage deviation ΔU_{dc}. When ΔU_{dc} is small, $K_{\mathrm{f}}^{\mathrm{DC}}$ is large, so that the power support of the MTDC system has a negligible influence on the DC voltage stability, thus alleviating the power deficit of the disturbed AC system. On the other hand, $K_{\mathrm{f}}^{\mathrm{DC}}$ is small when the ΔU_{dc} is large, and the MTDC system reduces the support power to maintain the voltage stability of the DC grid.

In combination with (13) and (14), the frequency droop coefficient K_{f} of the dynamic additional frequency control is defined as:

$$K_{\mathrm{f}}=(1-\gamma)K_{\mathrm{f}}^{\mathrm{AC}}+\gamma K_{\mathrm{f}}^{\mathrm{DC}} \quad (15)$$

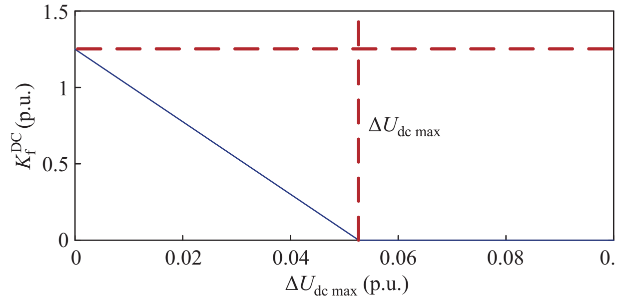

Fig. 6. DC frequency droop coefficient.

where γ represents the transition factor, which is defined in (16) and (17). n_1 is a positive integer. $\Delta U_{\mathrm{dc}\gamma1}$ is the start-up DC voltage deviation of γ, and $\Delta U_{\mathrm{dc}\gamma2}$ is the termination DC voltage deviation of γ.

$$\gamma=\begin{cases} 0 & \Delta U_{\mathrm{dc}}\le\Delta U_{\mathrm{dc}\gamma1} \\ \gamma' & \Delta U_{\mathrm{dc}\gamma1}<\Delta U_{\mathrm{dc}}\le\Delta U_{\mathrm{dc}\gamma2} \\ 1 & \Delta U_{\mathrm{dc}}>\Delta U_{\mathrm{dc}\gamma2}\end{cases} \quad (16)$$

$$\gamma'=\frac{1}{1+\left(\frac{\Delta U_{\mathrm{dc}\gamma2}-\Delta U_{\mathrm{dc}\gamma1}}{\Delta U_{\mathrm{dc}}-\Delta U_{\mathrm{dc}\gamma1}}-1\right)^{2n_1}} \quad (17)$$

The characteristics of the transition factor γ are shown in Fig. 7.

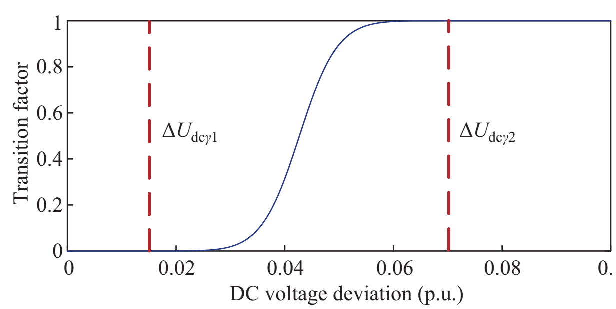

Fig. 7. Transition factor.

When the DC voltage deviation ΔU_{dc} is slightly larger than the start-up DC voltage deviation $\Delta U_{\mathrm{dc}\gamma1}$, the transition factor γ increases slowly from 0. As the DC voltage deviation ΔU_{dc} grows, γ increases rapidly from 0 to 1 and reaches 1 at the termination DC voltage deviation $\Delta U_{\mathrm{dc}\gamma2}$. According to (13)–(17), the characteristics of the droop coefficient K_{f} of the dynamic additional frequency control are shown in Fig. 8.

When the AC system disturbance is slight, the DC voltage deviation ΔU_{dc} is small, and the transition factor γ is close to 0. Therefore, the dynamic frequency droop coefficient K_{f} is consistent with the AC frequency droop coefficient $K_{\mathrm{f}}^{\mathrm{AC}}$. K_{f} increases rapidly as Δf increases; thus, the DC system increases the power support for the disturbed AC system. When the system disturbance is severe, Δf and ΔU_{dc} becomes large, and γ is close to 1. Under such a circumstance, K_{f} is consistent with the DC frequency droop coefficient $K_{\mathrm{f}}^{\mathrm{DC}}$, which decreases rapidly to avoid a large voltage deviation of the DC grid and enhance the MTDC system stability under strong frequency disturbance.

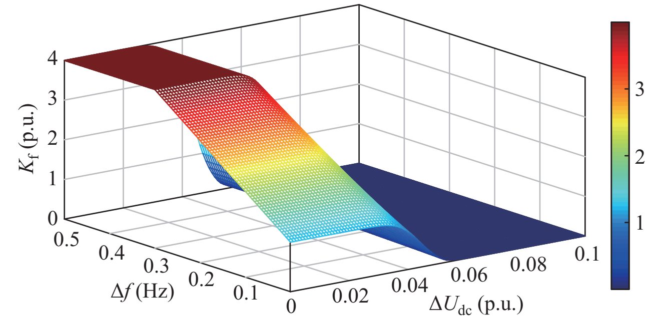

Fig. 8. The dynamic frequency droop coefficient.

The dynamic frequency droop coefficient combines the characteristics of the AC frequency droop coefficient with that of the DC frequency droop coefficient using a transition factor. By dynamically adjusting the frequency droop coefficient, the power compensation of the disturbed AC system is strengthened when the DC voltage deviation is small. The voltage stability of the MTDC system has higher priority when the DC voltage deviation is large. Thus, the coordinated control of AC system frequency regulation and MTDC system voltage stability is achieved.

B. Small Signal Stability Analysis

The simplified model in Fig. 9 can be used to analyze the stability of the dynamic additional frequency control.

The capacitance of the VSC satisfies:

$$C\frac{\mathrm{d}U_{\mathrm{dc}}}{\mathrm{d}t}=I_{\mathrm{dc}}-i_1 \tag{18}$$

where C represents the DC capacitance, I_{dc} represents the DC current, and i_1 represents the current flowing to the other VSCs.

The following can be derived from the AC side of the VSC:

$$L_{\mathrm{m}}\frac{\mathrm{d}i_{\mathrm{s}j}}{\mathrm{d}t}=-R_{\mathrm{s}}i_{\mathrm{s}j}+(U_{\mathrm{s}j}-U_{\mathrm{e}j}) \tag{19}$$

where R_{s} and L_{m} represent the equivalent resistance and

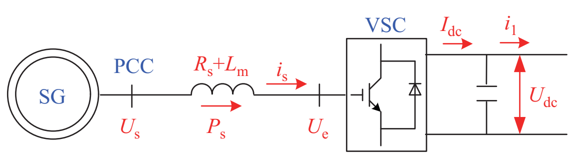

Fig. 9. Schematic diagram of VSC.

reactance, respectively, from the point of common coupling (PCC) to the VSC, i_{s} represents the AC current, U_{s} represents the voltage of the PCC, and U_{e} represents the AC voltage of the VSC; $j=a,b,c$.

The Park transformation is applied to (19), yielding:

$$\frac{\mathrm{d}}{\mathrm{d}t}\begin{pmatrix}i_d\\ i_q\end{pmatrix}=\frac{1}{L_{\mathrm{m}}}\begin{pmatrix}-R_{\mathrm{s}} & \omega L_{\mathrm{m}}\\ -\omega L_{\mathrm{m}} & -R_{\mathrm{s}}\end{pmatrix}\begin{pmatrix}i_d\\ i_q\end{pmatrix}+\frac{1}{L_{\mathrm{m}}}\begin{pmatrix}U_{\mathrm{s}d} & -U_{\mathrm{e}d}\\ U_{\mathrm{s}q} & -U_{\mathrm{e}q}\end{pmatrix} \tag{20}$$

In the steady-state, the d axis is consistent with the phase angle of the A-phase voltage of the PCC, i.e., $U_{\mathrm{s}q}=0$. If the losses of the reactor and converter are ignored, the active power of the AC and DC sides of the VSC are equal.

$$P_{\mathrm{s}}=\frac{3}{2}U_{\mathrm{s}d}i_d=U_{\mathrm{dc}}I_{\mathrm{dc}} \tag{21}$$

where P_{s} represents the active power exchanged between the VSC and AC system.

The motion equation of the generator rotor satisfies:

$$T_{\mathrm{J}}\frac{\mathrm{d}\omega}{\mathrm{d}t}=P_{\mathrm{m}}-P_{\mathrm{s}}-D(\omega-1) \tag{22}$$

where T_J represents the inertia time constant, ω represents the angular frequency, P_{m} represents the mechanical power of the prime mover, and D represents the damping coefficient.

The block diagram of the transfer function of the dynamic additional frequency control is shown in Fig. 10. The diagram is based on (18)–(22) and the vector control of the VSC. k_{p1} and k_{p2} are the proportional coefficients of the PI of the outer loop and inner loop, respectively. And k_{i1} and k_{i2} are the integral coefficients of the PI of the outer loop and inner loop, respectively. According to Fig. 10, the transfer function of the dynamic additional frequency control is:

$$G(s)=\frac{A(s)}{B(s)} \tag{23}$$

$$\begin{aligned}A(s)=\;&3Ck_{p1}k_{p2}K_{\mathrm{f}}K_{\mathrm{V}}U_{\mathrm{dc0}}U_{\mathrm{s}d0}\cdot s^3\\&+(3Ck_{i2}k_{p1}K_{\mathrm{f}}K_{\mathrm{V}}U_{\mathrm{dc0}}U_{\mathrm{s}d0}\\&+3Ck_{i1}k_{p2}K_{\mathrm{f}}K_{\mathrm{V}}U_{\mathrm{dc0}}U_{\mathrm{s}d0})\cdot s^2\\&+3Ck_{i1}k_{i2}K_{\mathrm{f}}K_{\mathrm{V}}U_{\mathrm{dc0}}U_{\mathrm{s}d0}\cdot s\end{aligned} \tag{24}$$

$$\begin{aligned}B(s)=\;&2CL_{\mathrm{m}}T_{\mathrm{J}}U_{\mathrm{dc0}}\cdot s^5+(2CDL_{\mathrm{m}}U_{\mathrm{dc0}}+2Ck_{p2}T_{\mathrm{J}}U_{\mathrm{dc0}}\\&+2CR_{\mathrm{s}}T_{\mathrm{J}}U_{\mathrm{dc0}}+3Ck_{p1}k_{p2}K_{\mathrm{V}}T_{\mathrm{J}}U_{\mathrm{dc0}}U_{\mathrm{s}d0})\cdot s^4\\&+(2CDk_{p2}U_{\mathrm{dc0}}+2CDR_{\mathrm{s}}U_{\mathrm{dc0}}+2Ck_{i2}T_{\mathrm{J}}U_{\mathrm{dc0}}\end{aligned}$$

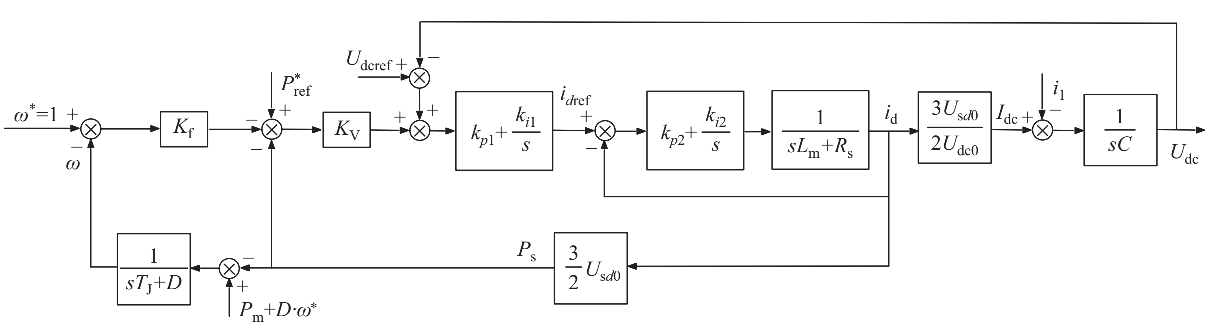

Fig. 10. Transfer function of the dynamic additional frequency control.

$$
\begin{aligned}
&+3k_{p1}k_{p2}T_{\mathrm{J}}U_{\mathrm{sd0}}+3CDk_{p1}k_{p2}K_{\mathrm{V}}U_{\mathrm{dc0}}U_{\mathrm{sd0}}\\
&+3Ck_{p1}k_{p2}K_{\mathrm{f}}K_{\mathrm{V}}U_{\mathrm{dc0}}U_{\mathrm{sd0}}\\
&+3Ck_{i2}k_{p1}K_{\mathrm{V}}T_{\mathrm{J}}U_{\mathrm{dc0}}U_{\mathrm{sd0}}\\
&+3Ck_{i1}k_{p2}K_{\mathrm{V}}T_{\mathrm{J}}U_{\mathrm{dc0}}U_{\mathrm{sd0}})\cdot s^3+(2CDk_{i2}U_{\mathrm{dc0}}\\
&+3Dk_{p1}k_{p2}U_{\mathrm{sd0}}+3k_{i2}k_{p1}T_{\mathrm{J}}U_{\mathrm{sd0}}+3k_{i1}k_{p2}T_{\mathrm{J}}U_{\mathrm{sd0}}\\
&+3CDk_{i2}k_{p1}K_{\mathrm{V}}U_{\mathrm{dc0}}U_{\mathrm{sd0}}\\
&+3CDk_{i1}k_{p2}K_{\mathrm{V}}U_{\mathrm{dc0}}U_{\mathrm{sd0}}\\
&+3Ck_{i2}k_{p1}K_{\mathrm{f}}K_{\mathrm{V}}U_{\mathrm{dc0}}U_{\mathrm{sd0}}\\
&+3Ck_{i1}k_{p2}K_{\mathrm{f}}K_{\mathrm{V}}U_{\mathrm{dc0}}U_{\mathrm{sd0}}\\
&+3Ck_{i1}k_{i2}K_{\mathrm{V}}T_{\mathrm{J}}U_{\mathrm{dc0}}U_{\mathrm{sd0}})\cdot s^2\\
&+(3Dk_{i2}k_{p1}U_{\mathrm{sd0}}+3Dk_{i1}k_{p2}U_{\mathrm{sd0}}+3k_{i1}k_{i2}T_{\mathrm{J}}U_{\mathrm{sd0}}\\
&+3CDk_{i1}k_{i2}K_{\mathrm{V}}U_{\mathrm{dc0}}U_{\mathrm{sd0}}\\
&+3Ck_{i1}k_{i2}K_{\mathrm{f}}K_{\mathrm{V}}U_{\mathrm{dc0}}U_{\mathrm{sd0}})\cdot s\\
&+3Dk_{i1}k_{i2}U_{\mathrm{sd0}} \qquad (25)
\end{aligned}
$$

The parameters of the control links are shown in Table I.

Figure 11(a) shows the root locus of the transfer function with the increase in K_{f}, and Fig. 11(b)–(f) show the distribution of the zeros and poles. The closed-loop transfer function has three zeros and five poles. As shown in Fig. 11(b) and (c), two zeros are located on the real axis of the left half-plane, and another is at the origin. As shown in Fig. 11(d), the two poles are initially located on the real axis of the left half-plane. With the increase in K_{f}, one converges to the remote zero point, and the other tends to the proximal one. In Fig. 11(e), the pole is located on the left of the imaginary axis and moves to the origin along the real axis. The three poles are always located on the left side of the imaginary axis; thus, there is no stability problem. As shown in Fig. 11(f), the two poles are located on the left half-plane, but they will cross the imaginary axis with an increase in K_{f}, resulting in the system's instability.

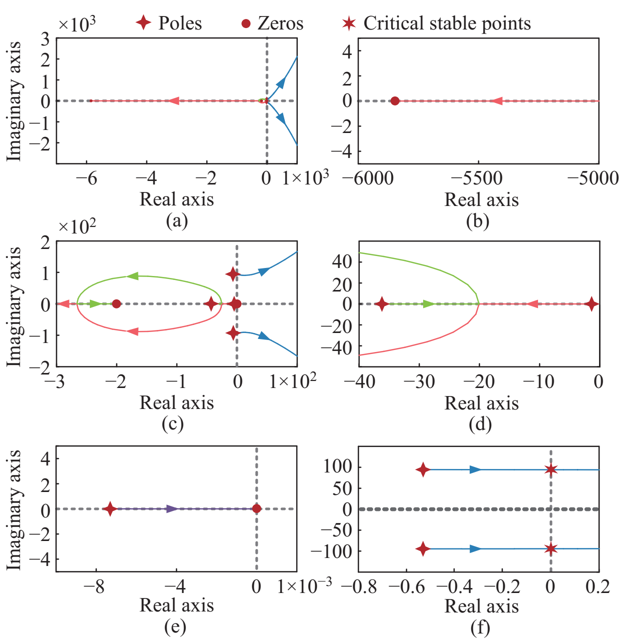

Fig. 11. Root locus of the dynamic additional frequency control. (a) Original figure. (b) Enlarged drawing 1. (c) Enlarged drawing 2. (d) Enlarged drawing 3. (e) Enlarged drawing 4. (f) Enlarged drawing 5.

TABLE I
PARAMETERS OF THE CONTROL LINKS

Parameter	Quantity
D	7.5 p.u.
T_J	6.234 s
K_{V}	0.5 p.u.
k_{p1}	0.01 p.u.
k_{i1}	100 p.u.
k_{p2}	0.5 p.u.
k_{i2}	100 p.u.
R_{s}	0.3142 Ω
L_{m}	0.021 H
U_{sd}	127.017 kV
U_{dc}	400 kV
C	1800 μF

When the two poles move to the imaginary axis, the system reaches the critical stable state, and the corresponding K_{f} is 20.4. Therefore, the stability range of the dynamic additional frequency control is:

$$0 < K_{\mathrm{f}} < 20.4 \qquad (26)$$

IV. DC Voltage Recovery Module

A. The Proportional Gain of the DC Voltage Recovery

The novel dynamic additional frequency control designs a DC voltage recovery module because the DC voltage deviates from the steady operating point when regulating the frequency. The DC voltage recovery module adds the product of the DC voltage deviation and proportional gain to the active power reference value. The VSCs connected to the normal AC systems participate in the DC grid voltage recovery after the disturbance.

The initial steady-state values can be calculated by (6)–(8), and do not need to be repeated here.

It can be obtained from the energy conservation equation after the dynamic additional frequency control has been implemented:

$$\sum_{i=1}^{n}\Delta P_i^1 = 0 \qquad (27)$$

The DC voltage droop control of VSC$_i$ satisfies:

$$K_{\mathrm{V}i}\left(\Delta P_i^0+\Delta P_i^1\right)+\left(\Delta U_{\mathrm{dc}i}^0+\Delta U_{\mathrm{dc}}^1\right)=0 \qquad (28)$$

where $i = 2, \cdots, n$.

If $E=\sum_{i=2}^{n}\frac{1}{K_{\mathrm{V}i}}$, (9), (27) and (28) yield:

$$\Delta U_{\mathrm{dc}}^1=\frac{-P_{\mathrm{loss}}+\Delta P_1^0+\Delta P_1^1-\sum_{i=2}^{n}\left(\frac{1}{K_{\mathrm{V}i}}\Delta U_{\mathrm{dc}i}^0\right)}{E} \qquad (29)$$

The ΔP_i^1 of VSC$_i$ is

$$\Delta P_i^1=-\Delta P_i^0-\frac{1}{K_{\mathrm{V}i}}\left(\Delta U_{\mathrm{dc}i}^0+\Delta U_{\mathrm{dc}}^1\right) \qquad (30)$$

After the DC voltage recovery module is implemented, the droop control of each converter shall satisfy (31):

$$\frac{K_{\mathrm{V}i}}{K_i+1}\left(\Delta P_i^0+\Delta P_i^1+\Delta P_i^2\right)+\left(\Delta U_{\mathrm{dc}i}^0+\Delta U_{\mathrm{dc}}^1+\Delta U_{\mathrm{dc}}^2\right)=0 \qquad (31)$$

where $\Delta P_i^2 = P_i^1 - P_i^2$, P_i^2 represents the steady-state active power of VSC$_i$ after DC voltage recovery, ΔU_{dc}^2 is the difference between the average DC voltage before and after DC voltage recovery, and $i = 2, \cdots, n$.

This is because the converter connected to the disturbed AC system does not participate in the DC voltage recovery, it operates in the fixed active power control mode, i.e., $\Delta P_i^2 = 0$. According to the energy conservation equation, the following applies:

$$\sum_{i=1}^{n} \Delta P_i^2 = 0 \tag{32}$$

Let $F = \sum_{i=2}^{n} \frac{K_i+1}{K_{\mathrm{V}i}}$, (9), (27), (31) and (32) are derived:

$$\Delta U_{\mathrm{dc}2} = \frac{-P_{\mathrm{loss}} + \Delta P_1^0 + \Delta P_1^1}{F} - \frac{\sum_{i=2}^{n}\left(\frac{K_i+1}{K_{\mathrm{V}i}} \times \Delta U_{\mathrm{dc}i}^0\right)}{F} - \Delta U_{\mathrm{dc}}^1 \tag{33}$$

$$\Delta P_i^2 = -\left(\Delta P_i^0 + \Delta P_i^1\right) - \frac{K_i+1}{K_{\mathrm{V}i}}\left(\Delta U_{\mathrm{dc}i}^0 + \Delta U_{\mathrm{dc}}^1 + \Delta U_{\mathrm{dc}}^2\right) \tag{34}$$

To achieve non-error recovery of the DC voltage, it is required that $\Delta U_{\mathrm{dc}}^2 = -\Delta U_{\mathrm{dc}}^1$, which means:

$$-P_{\mathrm{loss}} + \Delta P_1^0 + \Delta P_1^1 - \sum_{i=2}^{n}\left(\frac{K_i+1}{K_{\mathrm{V}i}}\Delta U_{\mathrm{dc}i}^0\right) = 0 \tag{35}$$

When the AC system frequency drops, the value of $-P_{\mathrm{loss}} + \Delta P_1^0 + \Delta P_1^1$ is positive, and the contribution of the converter with negative $\Delta U_{\mathrm{dc}i}^0$ to the DC voltage recovery is negative. Therefore, the corresponding converter $K_i + 1$ is set to 0 to counteract its negative effect on DC voltage recovery. In other words, this type of converter is switched to fixed active power control and does not participate in the DC voltage recovery. In contrast, if the frequency increases, the VSC with positive $\Delta U_{\mathrm{dc}i}^0$ is set $K_i + 1$ to 0 to not participate in the DC voltage recovery.

If the K_i of the converters participating in the DC voltage recovery are equal, then the theoretical value of the proportional gain of the DC voltage recovery module is:

$$K_{\mathrm{th}} = \frac{-P_{\mathrm{loss}} + \Delta P_1^0 + \Delta P_1^1}{\sum\left(\frac{1}{K_{\mathrm{V}i}}\Delta U_{\mathrm{dc}i}^0\right)} - 1 \tag{36}$$

B. Stable DC Voltage Recovery

When the DC voltage recovery module is implemented, the operating points of the droop control for the VSCs suddenly stop, causing the DC voltage and transmission power to significantly oscillate. When a Butterworth low-pass filter approximates the ideal low-pass filter, the smoothness can be easily adjusted [34]. A function similar to the Butterworth filter transfer function (short for Butterworth function) is proposed in (37) and (38) to avoid the oscillations, and the DC voltage recovery gain K is gradually increased from zero to the theoretical value calculated by (36) to complete the smooth connection of the DC voltage recovery module.

$$K = \begin{cases} 0 & t \le t_0 \\ K' & t_0 < t \le t_1 \\ K_{\mathrm{th}} & t > t_1 \end{cases} \tag{37}$$

$$K' = \frac{K_{\mathrm{th}}}{1 + \left(\frac{t_1 - t_0}{t - t_0} - 1\right)^{2N}} \tag{38}$$

where t_0 and t_1 are the start-up time and termination time of the DC voltage recovery, and N is a positive integer.

Figure 12 shows different forms of the DC voltage recovery gain. Compared with the DC voltage recovery gain that uses the theoretical value, the Butterworth function increases the buffer interval to weaken the impact. Moreover, compared with the DC voltage recovery gain that increases at a fixed slope, the derivative of the Butterworth function does not produce saltation at the beginning and end of the recovery period, ensuring smooth transitions between the states.

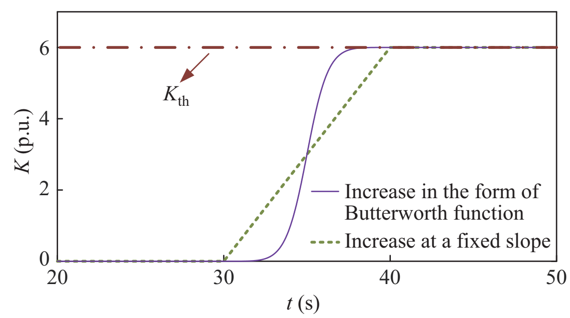

Fig. 12. The DC voltage recovery gain.

The premise of the DC voltage recovery module activation is that the VSC-MTDC system reaches a quasi-steady state, so it is necessary to determine whether the system parameters reach a quasi-steady state value. With active power P as the determining parameter, theoretically, when the differential $\mathrm{d}P/\mathrm{d}t$ of P is equal to 0, P reaches a steady state. The numerical calculation of $\mathrm{d}P/\mathrm{d}t$ is first needed to compute the differential values from multiple points, then take the average value, which is shown in (39):

$$\frac{\mathrm{d}P}{\mathrm{d}t} = \frac{1}{m}\sum_{i=0}^{m-1}\frac{P(n+m+i) - P(n+i)}{m} \tag{39}$$

where $P(n)$ is the sampling value of P at time t, $P(n+i)$ is the sampling value of P at time $t + i\Delta t$, and Δt is the sampling step length.

Sampling step length Δt is usually with the level of microseconds, $\mathrm{d}P/\mathrm{d}t$ is difficult to be equal to 0, so P can be considered to reach the steady state value when it meets the following conditions:

$$\left|\frac{\mathrm{d}P}{\mathrm{d}t}\right| \le M \tag{40}$$

where M is a tiny threshold, and 0.1 MW/s is used as the judgment boundary of the steady value of active power in this paper.

The time when the active power P satisfies (40) is taken as the time when the VSC reaches the quasi-steady. The dispatching center compares the steady state time uploaded by each VSC, and uses the latest time as the start-up time t_0 start the DC voltage recovery.

At the same time, when the interval between the start-up time and the termination time of the DC voltage recovery module is too short, the energy redistribution time of the VSC-MTDC system is insufficient, thus a large fluctuation peak will occur in the transition process. Therefore, it is necessary to set a longer time interval to avoid shocks during the transition process. Considering that the DC voltage recovery depends on the active power adjustment of the AC system connected to VSC, and the active power adjustment time of the generators is usually with the level of seconds [35], thus the time interval of the DC voltage recovery module adopted in this paper under the PSCAD/EMTDC is 10 s, that is $t_1 - t_0 = 10$ s.

The novel dynamic additional frequency control coordinates the DC voltage recovery modules of multiple converters, and the DC voltage recovery proportional gain increases in the form of the Butterworth function. Thus, the smooth transition from start-up to steady-state of the DC voltage recovery module is achieved, and the DC voltage of the MTDC system recovers without errors after the disturbance.

V. Case Study

A. Simulation Model

A four-terminal VSC-HVDC simulation model (Fig. 13) is implemented on PSCAD/EMTDC to verify the performance of the novel dynamic additional frequency control.

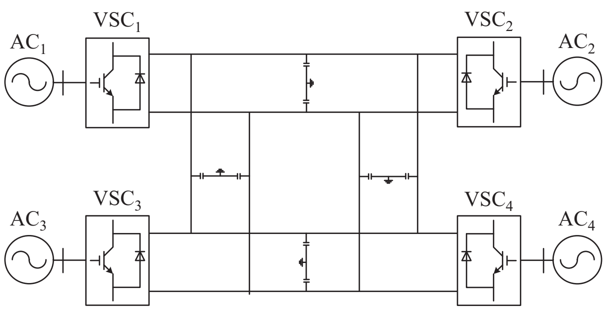

Fig. 13. Simulation model of the 4-terminal VSC-HVDC system.

The parameters of the different AC systems and the initial values of the VSCs are summarized in Table II.

TABLE II
Parameters of the AC/DC Hybrid Systems

Parameter	Area				Unit
	1	2	3	4	
f^*	50	50	50	50	Hz
U_{AC}	220	220	220	220	kV
S	1200	800	1500	900	MVA
P_{ref}	400	400	−500	−300	MW
U_{dcref}	400	400	400	400	kV
K_{V}	0.5	0.5	0.4	0.67	p.u.

U_{AC} is the effective value of the AC system line voltage, and S represents the capacities of the AC system. The resistance between the interconnected converters is 1.2 Ω.

B. Small Frequency Disturbance

At $t = 15$ s, the load of AC system 1 is suddenly increased by 100 MW. The changes in the frequency f_1 of AC system 1 and the DC voltage U_{dc1} of VSC_1 are depicted in Fig. 14.

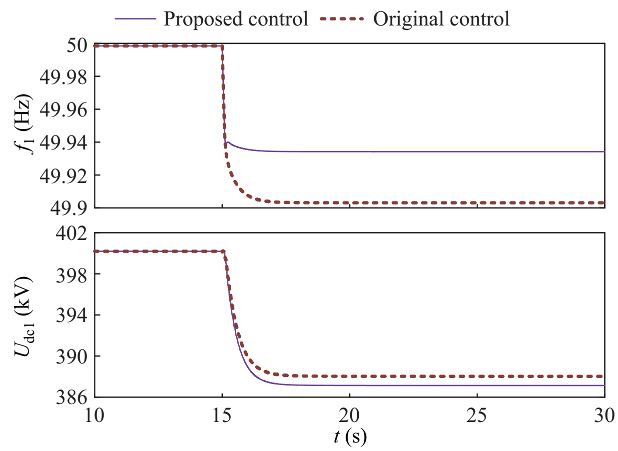

Fig. 14. Frequency of AC_1 and DC voltage of VSC_1 during a small disturbance.

f_1 drops from 50 Hz to 49.903 Hz under the original additional frequency control, and the frequency change Δf_1 is 0.097 Hz. In contrast, the frequency change Δf_1 in the system with the novel dynamic additional frequency control is 0.066 Hz, which is 31.96% less than that of the system with the original additional frequency control. The DC voltage change ΔU_{dc1} of VSC_1 is 13.05 kV, representing a 7.32% increase compared to the system with the original additional frequency control, whose change ΔU_{dc1} is 12.16 kV. The simulation results indicate that the proposed control strategy provides an effective improvement in the frequency deviation of AC system 1 at the cost of only a slight increase in the DC voltage.

When a small power imbalance occurs in the AC system, both the frequency deviation and the DC voltage changes are small; thus, the dynamic frequency droop coefficient K_{f} shows the characteristics of the AC frequency droop coefficient $K_{\mathrm{f}}^{\mathrm{AC}}$. The rapidly growing K_{f} enables the DC grid to provide more support power for AC system frequency regulation than the system with the original additional frequency control. In addition, the DC voltage deviation in the system with the novel dynamic additional frequency control is slightly larger than that in the original control system. In the case of a small disturbance, the novel dynamic additional frequency control can effectively decrease the frequency deviation of the disturbed AC system and has little influence on the DC grid, thus ensuring the stable operation of the MTDC system.

C. Large Frequency Disturbance

At $t = 15$ s, the load of AC system 1 is abruptly increased by 300 MW; the evolution of f_1, f_3 and U_{dc1} are depicted in Fig. 15.

The DC voltage of VSC_1 with the original additional frequency control is reduced from 400.19 kV to 359.68 kV, ΔU_{dc1} is 40.51 kV, and the DC voltage drop ratio is 10.12%. The DC voltage drop ratio exceeds the safe operating limit of the DC grid, as specified by the national standard. This will trigger the DC grid relay protection action, threatening the stability of the MTDC system. In addition, in AC system 3, the power support for AC system 1 causes f_3 to drop from 50 Hz to 49.653 Hz. The frequency variation Δf_3 is 0.347 Hz,

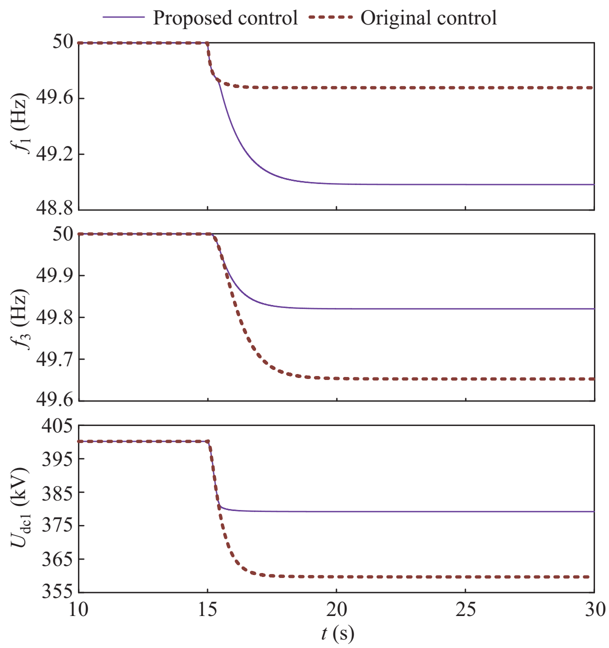

Fig. 15. Frequency of AC_1, AC_3, and DC voltage of VSC_1 in a large disturbance.

and the frequency stability of the normal AC system is significantly decreased. By adopting the novel dynamic additional frequency control, the DC voltage change ΔU_{dc1} decreases from 40.51 kV to 20.98 kV, so that the operating condition of the DC grid is significantly improved. Moreover, the frequency deviation Δf_3 is 0.179 Hz compared to 0.347 Hz, and the influence on the normal AC system is considerably reduced.

When a large frequency disturbance occurs in the AC system, both the frequency deviation and the DC voltage variation are large; thus, the characteristics of K_{f} are in agreement with that of the DC frequency droop coefficient $K_{\mathrm{f}}^{\mathrm{DC}}$. Compared with the original additional frequency control, K_{f} decreases rapidly as ΔU_{dc} increases, which avoids the instability of the MTDC system resulting from the excessive power support. In the case of a large disturbance, the novel dynamic additional frequency control gives priority to maintaining the stability of the DC voltage, which avoids critical damage to the entire AC and DC system caused by a large power disturbance of the local AC system.

D. DC Voltage Recovery

At $t = 30$ s, the DC voltage recovery is implemented due to the large frequency disturbance. VSC_1, which is connected to the disturbed AC system, does not participate in DC voltage recovery, and its control mode changes to fixed active power control. The initial DC voltage deviation $\Delta U_{\mathrm{dc2}}^0$ of VSC_2 is -0.34 kV. According to (35), the contribution of VSC_2 to the DC voltage recovery is negative. Therefore, the DC voltage recovery gain K_2 is set to -1 so that VSC_2 acts as a fixed active power control. The initial DC voltage deviations $\Delta U_{\mathrm{dc3}}^0$ and $\Delta U_{\mathrm{dc4}}^0$ of VSC_3 and VSC_4 are both positive. Therefore, the theoretical value calculated by (36) is assigned to the proportional gain of the DC voltage recovery module of VSC_3 and VSC_4 for DC voltage recovery.

Table III shows the comparison of the theoretical values and system simulation results of the DC voltage of the four VSCs. The results indicate that the relative error between the theoretical value and the actual value of the DC voltage of each VSC in the initial state, after the disturbance, and after voltage recovery does not exceed 0.1%. Moreover, the theoretical and actual values of ΔU_{dc}^1 are 20.86 kV and 20.85 kV, respectively, and those of ΔU_{dc}^2 are -20.86 kV and -21.16 kV, respectively. The relative errors between them are less than 1.5%, indicating the high accuracy of the theoretical calculation of the DC voltage recovery module.

TABLE III
DC VOLTAGE OF THE MTDC SYSTEM

System state	Numerical type	U_{dc1} (kV)	U_{dc2} (kV)	U_{dc3} (kV)	U_{dc4} (kV)
Before disturbance	theoretical value	400.27	400.34	399.00	399.22
	actual value	400.19	400.26	398.92	399.14
After disturbance	theoretical value	379.41	379.49	378.14	378.37
	actual value	379.20	379.47	378.07	378.35
After recovery	theoretical value	400.27	400.34	399.00	399.22
	actual value	400.35	400.60	399.28	399.53

According to (36), Tables II, III and Fig. 15, the theoretical value of the proportional gain K_{th} of the DC voltage recovery module is 33.18. Four modes are compared during the DC voltage recovery, i.e., K assigned to K_{th} (mode 1), K increasing to K_{th} from 0 with a fixed slope (mode 2), K increasing to K_{th} from 0 in the form of the Butterworth function described in (37) and (38) (mode 3), and the strategy proposed in [32] (mode 4).

P_2, P_3 and P_4 in Fig. 16 represent the active power transmitted by VSCs 2, 3, and 4, respectively. After applying the novel dynamic additional frequency control, the DC voltage U_{dc1} of VSC_1 recovers from 379.20 kV to 400.35 kV. The VSC_2 does not participate in DC voltage recovery and operates in the fixed active power control mode. Thus, P_2 remains invariant at 441.05 MW. In addition, P_3 decreases from -445.18 MW to -437.53 MW, while P_4 increases from -267.52 MW to -275.35 MW. When implementing the strategy in [32], U_{dc1}

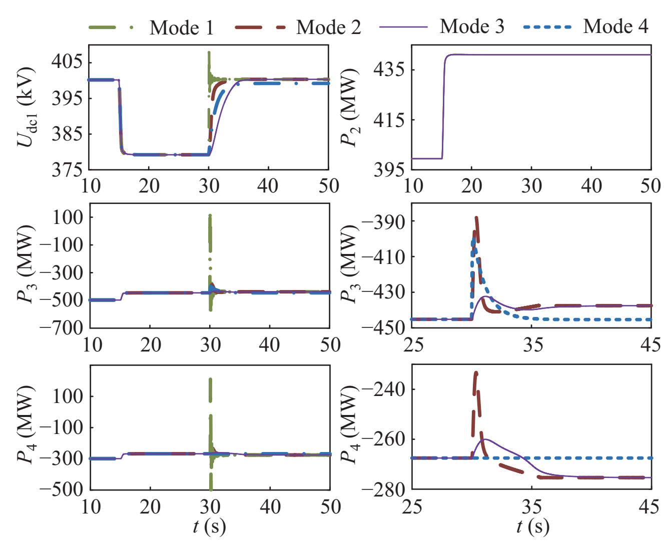

Fig. 16. DC voltage and real power in the DC voltage recovery process.

recovers to 399.22 kV, P_2 and P_4 remain constant, and P_3 converges to -445.18 MW again after violent fluctuation.

As shown in Fig. 16, modes 1, 2 and 3 have recovered their DC voltages to their initial values. Although mode 4 also realizes DC voltage recovery, U_{dc1} cannot recover to the initial value when VSC_3 operates in the fixed DC voltage control mode. In addition, mode 1 instantaneously breaks the balance of the control structure of the MTDC system, causing strong oscillations of the DC voltage U_{dc1} and active powers P_3 and P_4, while mode 4 results in a strong impact on P_3. In the four types of DC voltage recovery processes, mode 3 provides the least power fluctuations and smoothest recovery of the DC voltage.

The novel dynamic additional frequency control utilizes multiple converters to coordinate the DC voltage recovery. The proportional gain of the DC voltage recovery module is designed to perform DC voltage recovery without error. Meanwhile, the DC voltage recovery gain gradually increases with the Butterworth function, to ensure a smooth transition between the states before and after the DC voltage recovery.

E. The Performance after the Outage of VSC

At $t = 15$ s, VSC_4 is suddenly blocked. And when $t = 30$ s, the DC voltage recovery modules starts. The changes in U_{dc3}, P_1, P_2 and P_3 are depicted in Fig. 17.

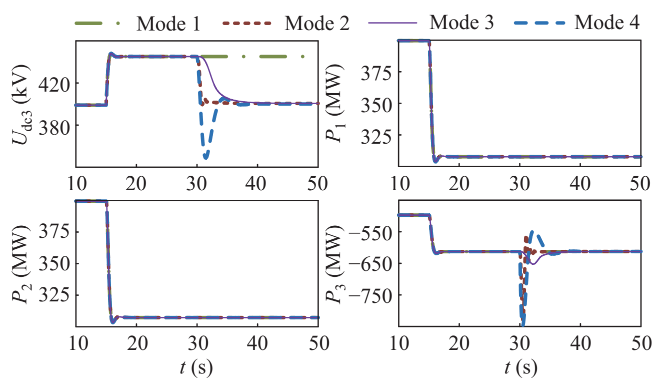

Fig. 17. DC voltage and real power after the outage of VSC_4.

The frequency support part of the proposed strategy is to control the unbalanced active power transmitted from the disturbed AC system to the DC grid. The unbalanced power caused by VSC_4 blocking is fixed, each VSC automatically allocates according to its droop coefficient, and the frequency support control does not need to be activated. The DC voltage module is put into use after the system reaches a transient steady state, to recover the DC voltage. Mode 1 represents the original droop control [36], and the other three modes are defined in Section V-D.

After VSC_4 blocking, P_1, P_2, P_3 are changed from 399.62 MW, 399.47 MW and -497.30 MW to 307.70 MW, 307.28 MW and -612.79 MW, respectively. And U_{dc3} is changed from 398.92 kV to 445.12 kV. The DC voltage deviation ΔU_{dc3} under the original droop control (mode 1) is 46.20 kV, which seriously threatens the system safety. Therefore, the DC voltage recovery module is necessary under such conditions. Because both the $\Delta U_{\mathrm{dc1}}^0$ and $\Delta U_{\mathrm{dc2}}^0$ are less than 0, VSC_1 and VSC_2 do not participate in the DC voltage recovery in mode 2 and mode 3, only VSC_3 undertakes the task of the DC voltage recovery. U_{dc3} recovers from 445.12 kV to 399.18 kV after implementing the dynamic additional frequency control strategy. And U_{dc3} recovers to 399.18 kV in mode 4. In addition, similar to the results in Section V-D, compared with mode 2 and mode 4, the proposed strategy using the Butterworth function to increase the DC voltage recovery gain can recover the DC voltage at a cost with smaller fluctuations.

Figure 18 shows the d-axis current i_{d3} of VSC_3 when the outer-loop PI controller adopts different bound values. The purpose of adding bound values to the PI controller is to restrain overshoot and improve transient performance. In this paper, the parameter tuning methods of [33] and [37] are used to determine the limiting amplitude of the PI controller. According to the converter capacity, the AC current of the grid side is calculated, and the Park transformation is utilized to obtain the d-axis current from the AC current value. Then 1.5 times the d-axis current is taken as the bound value of the outer-loop PI controller $i_{d\mathrm{lim}}$, which is 7.5 p.u. according to the computation. It can be seen from Fig. 18 that when $i_{d\mathrm{lim}}$ is smaller than the bound value, for example 6.2 p.u. and 6.3 p.u., i_{d3} becomes oscillatory. When $i_{d\mathrm{lim}}$ is set at 7.5 p.u. or 10 p.u., the system responses are identical and i_{d3} smoothly converges to the stable value. The simulation results in Fig. 18 verify the suitability of the bound value of the outer-loop PI controller.

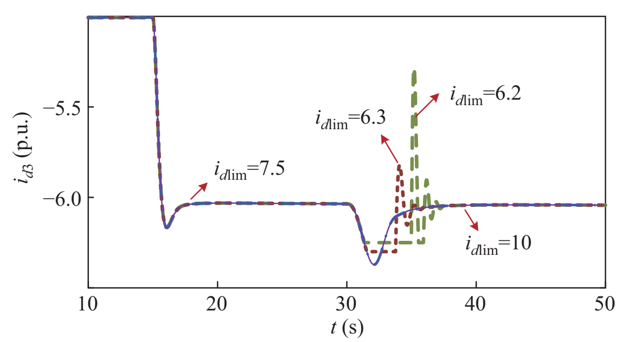

Fig. 18. i_{d3} with different limit of PI controller.

F. The Performance with Time Varying Load

At $t = 15$ s, AC system 1 is connected with a dynamic resistance which decreases linearly with time to simulate the continuous disturbance. The resistance is reduced from 1000 Ω to 200 Ω at a speed of 40 Ω/s. The response of the VSC-MTDC system is depicted in Fig. 19. i_{dref3} is the output of the d-axis outer-loop PI controller of VSC_3.

During 10–15 s, the VSC-MTDC system operates in steady state 1 as shown in Fig. 3, when each VSC only relies on the droop control to maintain system power balance.

After 15 s, AC_1 is connected to a dynamic load. The frequency control module of VSC_1 is activated, and the droop control is still used in other stations. It can be seen from Fig. 19, when the dynamic resistance is large, in other words, the dynamic load is small, the frequency deviation of the disturbed AC system with the dynamic additional frequency

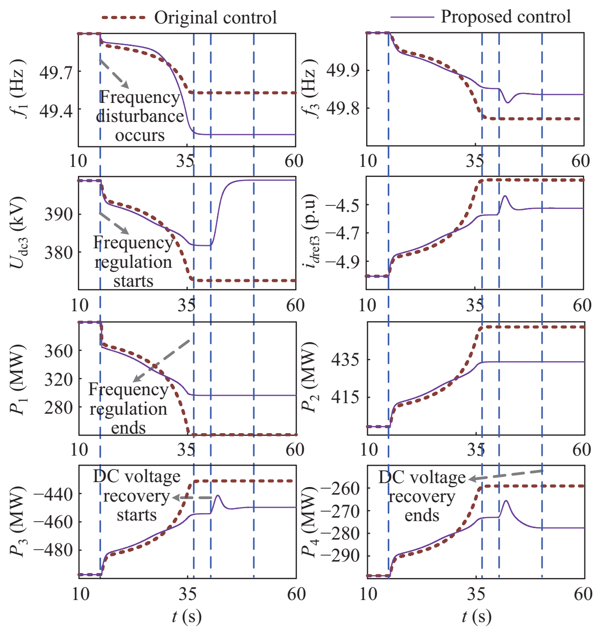

Fig. 19. DC voltage and real power when the load varies with time.

control is smaller than that with the original control. Under such a scenario, the proposed control strategy assigns a higher priority to improving the frequency of the disturbed AC system. So, the DC grid voltage deviation and the frequency of the normal AC system will be slightly larger, thus providing more power support. With the decrease of the dynamic resistance, the dynamic additional frequency control turns to preferentially maintain the stability of DC grid voltage, and the speed and amplitude of the DC voltage drop obviously decreases.

At 35 s, the dynamic resistance change process ends, and the state variables of VSC-MTDC system gradually reach the steady state, corresponding to steady state 2 in Fig. 3. Then, the DC voltage recovery process starts when the system reaches steady state as judged by (39) and (40). VSC_1 is changed to operate in the fixed active power mode. Due to the negative initial DC voltage deviation, VSC_2 does not participate in the DC voltage recovery and also operates in the fixed active power mode. VSC_3 and VSC_4 activate the DC voltage recovery module on the basis of the droop control module, to achieve the smooth and non-error recovery of the DC voltage.

VI. Conclusion

When a VSC-MTDC system utilizes the original additional frequency control to provide frequency support for a disturbed AC system, the stability of the DC voltage is often not considered, potentially resulting in large fluctuations in the DC voltage. Therefore, a novel VSC-MTDC dynamic additional frequency control strategy with DC voltage recovery ability is proposed in this paper.

1) The dynamic frequency droop coefficient is adaptively adjusted according to the frequency and DC voltage. In a small frequency disturbance, the dynamic frequency droop coefficient is large and the DC grid meets the power requirements of the disturbed AC system. In a large power disturbance, the dynamic frequency droop coefficient is small and the DC grid gives priority to maintaining the DC voltage stability. Thus, the novel dynamic additional frequency control provides a strong and reliable DC grid, as well as good support to the interconnected AC grids.

2) The DC voltage recovery method based on multi-converter coordination can realize smooth and non-error DC voltage of the MTDC system recovery after the frequency regulation. The proposed method recovers the DC voltage to the rated value, which improves the stable operation of the DC grid. Meanwhile, this method only needs to communicate once when calculating the DC voltage recovery gain, and has little dependence on communication facilities.

3) The simulation results demonstrate that the dynamic additional frequency control can adapt to power disturbances with different severities and maintain the DC voltage in a relatively stable state when regulating the frequency. The DC voltage recovery module is able to perform smooth and non-error recovery of the DC voltage after the disturbance.

Note that this paper focuses on the AC system and the VSCs when analyzing the small-signal stability of the proposed additional control and neglects the DC systems, whose current is treated as disturbance. Thus, a further study considering the DC systems and the small-signal stability analysis of the whole VSC-MTDC system should be undertaken. In addition, the frequency regulation can be enhanced by making full use of the rotating reserves of the wind turbines since the wind power penetration has dramatically increased in the past decades. The DC voltage recovery can also be improved by decentralizing and coordinating the multi-converter voltage control ability, which requires less communication burden from the system.

Appendix

The parameters of the dynamic frequency control module are shown in Table AI.

TABLE AI
Parameters of Dynamic Frequency Control Module

Parameter	Quantity
$K^{\text{AC}}_{\text{fmax}}$	4 p.u.
$K^{\text{AC}}_{\text{f0}}$	1.25 p.u.
$\Delta f_{\max}$	0.3 Hz
$K^{\text{DC}}_{\text{fmin}}$	0 p.u.
$K^{\text{DC}}_{\text{f0}}$	1.25 p.u.
ΔU_{dcmax}	0.055 p.u.
$\Delta U_{\text{dc}\gamma 1}$	0.015 p.u.
$\Delta U_{\text{dc}\gamma 2}$	0.07 p.u.
n_1	2
N	2

References

[1] A. Moharana and P. K. Dash, "Input-output linearization and robust sliding-mode controller for the VSC-HVDC transmission link," *IEEE Transactions on Power Delivery*, vol. 25, no. 3, pp. 1952–1961, Jul. 2010.

[2] L. Xiong, X. Liu, Y. Liu and F. Zhuo, "Modeling and stability issues of voltage-source converter-dominated power systems: A review," *CSEE Journal of Power and Energy Systems*, vol. 8, no. 6, pp. 1530–1549, Nov. 2022.

[3] S. Debnath, J. C. Qin, B. Bahrani, M. Saeedifard, and P. Barbosa, "Operation, control, and applications of the modular multilevel converter: A review," *IEEE Transactions on Power Electronics*, vol. 30, no. 1, pp. 37–53, Jan. 2015.

[4] I. M. Sanz, B. Chaudhuri, and G. Strbac, "Inertial response from offshore wind farms connected through DC grids," *IEEE Transactions on Power Systems*, vol. 30, no. 3, pp. 1518–1527, May 2015.

[5] K. Sun, H. Xiao and Y. Liu, "Optimized allocation method of the VSC-MTDC system for frequency regulation reserves considering ancillary service cost," *CSEE Journal of Power and Energy Systems*, vol. 8, no. 1, pp. 53–63, Jan. 2022.

[6] Y. F. Wen, J. P. Zhan, C. Y. Chung, and W. Y. Li, "Frequency stability enhancement of integrated AC/VSC-MTDC systems with massive infeed of offshore wind generation," *IEEE Transactions on Power Systems*, vol. 33, no. 5, pp. 5135–5146, Sep. 2018.

[7] D. G. Xu, Y. C. Liu, and J. Wu, "Review on control strategies of multi-terminal direct current transmission system," *Transactions of China Electrotechnical Society*, vol. 30, no. 17, pp. 1–12, Dec. 2015.

[8] B. Yang, L. Jiang, T. Yu, H. C. Shu, C. K. Zhang, W. Yao, and Q. H. Wu, "Passive control design for multi-terminal VSC-HVDC systems via energy shaping," *International Journal of Electrical Power & Energy Systems*, vol. 98, pp. 496–508, Jun. 2018.

[9] B. Yang, L. Jiang, W. Yao, and Q. Wu, "Perturbation observer based adaptive passive control for damping improvement of multi-terminal voltage source converter-based high voltage direct current systems," *Transactions of the Institute of Measurement and Control*, vol. 39, no. 9, pp. 1409–1420, Sept. 2017.

[10] H. F. Li, C. R. Liu, G. Y. Li, and R. Iravani, "An enhanced DC voltage droop-control for the VSC–HVDC grid," *IEEE Transactions on Power Systems*, vol. 32, no. 2, pp. 1520–1527, Mar. 2017.

[11] N. R. Chaudhuri, R. Majumder, and B. Chaudhuri, "System frequency support through multi-terminal DC (MTDC) grids," *IEEE Transactions on Power Systems*, vol. 28, no. 1, pp. 347–356, Feb. 2013.

[12] T. M. Haileselassie and K. Uhlen, "Primary frequency control of remote grids connected by multi-terminal HVDC," in *Proceeding of IEEE PES General Meeting*, Minneapolis, MN, USA, 2010, pp. 1–6.

[13] O. D. Adeuyi, M. Cheah-Mane, J. Liang, and N. Jenkins, "Fast frequency response from offshore multiterminal VSC–HVDC schemes," *IEEE Transactions on Power Delivery*, vol. 32, no. 6, pp. 2442–2452, Dec. 2017.

[14] W. Y. Wang, Y. Li, Y. J. Cao, U. Häger, and C. Rehtanz, "Adaptive droop control of VSC-MTDC system for frequency support and power sharing," *IEEE Transactions on Power Systems*, vol. 33, no. 2, pp. 1264–1274, Mar. 2018.

[15] C. Q. Du, E. Agneholm, and G. Olsson, "Comparison of different frequency controllers for a VSC-HVDC supplied system," *IEEE Transactions on Power Delivery*, vol. 23, no. 4, pp. 2224–2232, Oct. 2008.

[16] K. Rouzbehi, W. Y. Zhang, J. I. Candela, A. Luna, and P. Rodriguez, "Unified reference controller for flexible primary control and inertia sharing in multi-terminal voltage source converter-HVDC grids," *IET Generation, Transmission & Distribution*, vol. 11, no. 3, pp. 750–758, Feb. 2017.

[17] Y. J. Li, X. Zhao, and K. P. Wong, "Advanced control strategies of PMSG-based wind turbines for system inertia support," *IEEE Transactions on Power Systems*, vol. 32, no. 4, pp. 3027–3037, Jul. 2017.

[18] Y. J. Li, Z. Xu, J. Østergaard, and D. J. Hill, "Coordinated control strategies for offshore wind farm integration via VSC-HVDC for system frequency support," *IEEE Transactions on Energy Conversion*, vol. 32, no. 3, pp. 843–856, Sep. 2017.

[19] R. K. Ze, X. Y. Li, and D. L. Ying, "A frequency stability control strategy for interconnected VSC-MTDC transmission system," *Power System Technology*, vol. 38, no. 10, pp. 2729–2734, Dec. 2014.

[20] B. Silva, C. L. Moreira, L. Seca, Y. Phulpin, and J. A. P. Lopes, "Provision of inertial and primary frequency control services using offshore multiterminal HVDC networks," *IEEE Transactions on Sustainable Energy*, vol. 3, no. 4, pp. 800–808, Oct. 2012.

[21] M. Zhou, J. Xu, and Y. Z. Sun, "Coordinated control restraining wind power fluctuation of VSC-MTDC," *Electric Power Automation Equipment*, vol. 36, no. 12, pp. 29–35, Dec. 2016.

[22] W. Y. Wang, Y. Li, Y. J. Cao, Z. W. Xu, and Y. Tan, "Adaptive droop control strategy participating in power grid frequency regulation for VSC-MTDC transmission system," *Automation of Electric Power Systems*, vol. 41, no. 13, pp. 142–149, 161, Jul. 2017.

[23] J. Dai, Y. Phulpin, A. Sarlette, and D&. Ernst, "Coordinated primary frequency control among non-synchronous systems connected by a multi-terminal high-voltage direct current grid," *IET Generation, Transmission & Distribution*, vol. 6, no. 2, pp. 99–108, Feb. 2012.

[24] A. Kirakosyan, E. F. El-Saadany, M. S. El Moursi, and K. A. Hosani, "DC voltage regulation and frequency support in pilot voltage droop-controlled multiterminal HVdc systems," *IEEE Transactions on Power Delivery*, vol. 33, no. 3, pp. 1153–1164, Jun. 2018.

[25] J. Van de Vyver, J. D. M. De Kooning, B. Meersman, L. Vandevelde, and T. L. Vandoorn, "Droop control as an alternative inertial response strategy for the synthetic inertia on wind turbines," *IEEE Transactions on Power Systems*, vol. 31, no. 2, pp. 1129–1138, Mar. 2016.

[26] M. Y. Guan, J. Z. Cheng, C. Wang, Q. R. Hao, W. L. Pan, J. Zhang, and X. Zheng, "The frequency regulation scheme of interconnected grids with VSC-HVDC links," *IEEE Transactions on Power Systems*, vol. 32, no. 2, pp. 864–872, Mar. 2017.

[27] J. B. Zhu, C. D. Booth, G. P. Adam, A. J. Roscoe, and C. G. Bright, "Inertia emulation control strategy for VSC-HVDC transmission systems," *IEEE Transactions on Power Systems*, vol. 28, no. 2, pp. 1277–1287, May 2013.

[28] Y. J. Cao, W. Y. Wang, Y. Li, Y. Tan, C. Chen, L. He, U. Häger, and C. Rehtanz, "A virtual synchronous generator control strategy for VSC-MTDC system," *IEEE Transactions on Energy Conversion*, vol. 33, no. 2, pp. 750–761, Jun. 2018.

[29] R. Wang, L. J. Chen, T. W. Zheng, and S. W. Mei, "VSG-based adaptive droop control for frequency and active power regulation in the MTDC system," *CSEE Journal of Power and Energy Systems*, vol. 3, no. 3, pp. 260–268, Sep. 2017.

[30] A. E. Leon, "Short-Term frequency regulation and inertia emulation using an MMC-based MTDC system," *IEEE Transactions on Power Systems*, vol. 33, no. 3, pp. 2854–2863, May 2018.

[31] B. Yang, T. Yu, X. S. Zhang, L. N. Huang, H. C. Shu, and L. Jiang, "Interactive teaching-learning optimiser for parameter tuning of VSC-HVDC systems with offshore wind farm integration," *IET Generation, Transmission & Distribution*, vol. 12, no. 3, pp. 678–687, Feb. 2018.

[32] Z. C. Yuan, Z. L. Wu, Q. Jin, S. G. Jiang, and Y. Huang, "Frequency stabilization control strategy with DC voltage secondary regulation of VSC-MTDC based interconnected systems," *Automation of Electric Power Systems*, vol. 42, no. 23, pp. 9–13, 19, Jul. 2018.

[33] W. W. Wang, H. J. Yin, and L. Guan, "Parameter setting for double closed-loop vector control of voltage source PWM rectifier," *Transactions of China Electrotechnical Society*, vol. 25, no. 2, pp. 67–72, 79, Feb. 2010.

[34] A. S. Ali, A. G. Radwan, and A. M. Soliman , "Fractional order Butterworth filter: active and passive realizations," *IEEE Journal on Emerging and Selected Topics in Circuits and Systems*, vol. 3, no. 3, pp. 346–354, Sep. 2013.

[35] J. Z. Liu, Q. Yao, Y. Liu, and Y. Hu, "Wind farm primary frequency control strategy based on wind & thermal power joint control," *Proceedings of the CSEE*, vol. 37, no. 12, pp. 3462–3469, 3674, Jun. 2017.

[36] T. M. Haileselassie and K. Uhlen , "Impact of DC line voltage drops on power flow of MTDC using droop control," *IEEE Transactions on Power Systems*, vol. 27, no. 3, pp. 1441–1449, Aug. 2012.

[37] A. C. Xue, J. Y. Geng, R. H. Liu, C. S. Zhao, Q. Wang, and T. S. Bi, "Impact of limiter on output characteristics of DFIG during fault," *Electric Power Automation Equipment*, vol. 37, no. 10, pp. 29–33, 56, Oct. 2017.

Chongru Liu (M'10–SM'15) received B.S., M.S. and Ph.D. degrees in Electrical Engineering from Tsinghua University, Beijing, China. She was a visiting professor at the University of Hong Kong from 2009 to 2010, and she was a visiting professor at Washington State University from 2010 to 2011. She is currently a Professor in the School of Electrical and Electronic Engineering, North China Electric Power University. She is a member of the National Power System Management and Information Exchange Standardization Committee of China. She is a member of Beijing Nova and supported by the program of New Century Excellent Talents in University. Her research interests include analysis, simulation and control of AC/DC hybrid systems.

Haoyu Liu received a B.S. degree in Electrical Engineering from North China Electric Power University, Beijing, China, where he is currently pursuing a Ph.D. degree. His research interests include coordination control and stability analysis of VSC-MTDC.

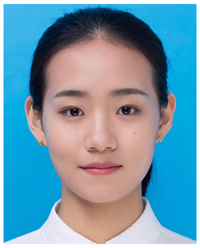

Siwen Jiang (S'20) received a B.S. degree in Electrical Engineering from North China Electric Power University, Beijing, China, in 2019. Her research interests include Mathematical analysis and suppression strategy of subsynchronous oscillation of PMSG.

Le Zheng (M'12) received B.S. and Ph.D. degrees in Electrical Engineering from Tsinghua University, Beijing, China, in 2011 and 2017, respectively. He was a Postdoctoral Research Fellow at Stanford University from 2017 to 2019. He is currently a faculty member of the North China Electric Power University, Beijing, China. His current research interests include stability and control of power electronics dominated power systems and renewable energy conversion systems, and machine learning applications in power systems.